Non-localized receptivity of boundary layers

By J. D. CROUCH†

Naval Research Laboratory, Washington, DC, USA

A perturbation scheme is developed to analyse the disturbance field produced by acoustic forcing over a flat plate with non-localized surface irregularities. Both the amplitude of the forcing and the height of the irregularity are assumed to be small. At first order, two modes are calculated: a Stokes mode resulting from the acoustic forcing, and a wall mode resulting from the surface irregularity. These modes interact at second order to produce a forced travelling wave with the frequency of the acoustic wave and a wavenumber associated with the surface irregularity. Streamwise variations in the mean flow mediate a distributed energy transfer between the forced mode and the eigenmode. Sufficiently far downstream, the forced-mode amplitude becomes small and the total disturbance is dominated by the resulting eigenmode. Receptivity amplitudes, expressed in terms of effective branch I values, are $O(10)$ for a broad range of surface wavenumbers.

1. Introduction

The process of laminar–turbulent transition in boundary layers has been linked to a sequence of instabilities. The streamwise evolution of these instabilities depends on their initial amplitudes, which are given as inputs in the stability analysis. To determine the initial disturbance amplitudes, boundary-layer receptivity studies attempt to describe the mechanisms for the induction of free-stream disturbances into the boundary layer. In general, the free-stream disturbances considered are classified as either acoustic or vortical (Goldstein & Hultgren 1989; Kerschen 1989). Acoustic disturbances are long-wavelength pressure perturbations that propagate through the fluid, while vortical disturbances are convected by the free stream. Receptivity mechanisms provide the necessary conversion of the long-wave free-stream disturbances into short-wave disturbances characteristic of the linear eigenmodes.

Early analytical studies of receptivity made use of a forced Orr–Sommerfeld equation to describe the induction of free-stream disturbances into the boundary layer (Mack 1975; Rogler & Reshotko 1975; Tam 1981). These models do not provide a means for rescaling the free-stream disturbance wavelength into scales associated with Tollmien–Schlichting (TS) waves. The scale-conversion process is activated by the interaction of a disturbance with flows generated by geometries containing small lengthscales. More recent theoretical studies have used asymptotic methods to investigate the receptivity associated with rapid changes in the mean flow. The focus has been on localized disturbances from either the leading edge or changes in wall geometry, including local roughness (Goldstein 1983; 1985). These analyses provide the necessary scale conversion and show a significant level of receptivity resulting

† Present address: Boeing Commercial Airplane Group, Seattle, WA 98124-2207, USA.

from the local geometric perturbations. Experimental results of Leehey & Shapiro (1980) are in general agreement with Goldstein & Hultgren's (1987) results for receptivity at the leading-edge juncture. The experiment of Aizin & Polyakov (1979) demonstrates that a thin strip of Mylar tape provides the necessary scale conversion for capturing acoustic free-stream disturbances. Their receptivity coefficients are in good agreement with the theory of Goldstein (1985).

Other experiments suggest that non-localized irregularities play a role in the receptivity process (Corke, Bar Sever & Morkovin 1986; Reshotko 1984). Wall roughness, for example, can be a source of short-wave disturbances within the boundary layer. When the roughness height is large, the disturbances are so strong that they lead to a 'by-pass' transition (Reshotko 1984). Small roughness heights, however, produce weak stationary disturbances (with zero phase speed). Reshotko (1976) suggested that these disturbances may be involved in the early development of eigenmodes. In the experiment of Corke *et al* (1986), distributed roughness had a dramatic affect on the early development of TS waves. They attribute this effect in part to low-inertia fluid between the surface protuberances; this fluid responds more readily than higher-inertia fluid to free-stream disturbances.

The present paper presents an analysis for acoustic receptivity of boundary layers over surfaces with non-localized irregularities. These irregularities may appear as non-uniformities in distributed roughness or as mild waviness of an otherwise smooth surface. The analysis captures the lengthscale conversion essential to acoustic receptivity. A perturbation scheme provides a decoupling of the relevant disturbance modes. At first order, two modes are calculated: a Stokes mode resulting from the acoustic forcing, and a wall mode resulting from the surface irregularity. These modes then interact at second order to produce a travelling wave with the acoustic frequency and a wavenumber associated with the surface perturbation. Streamwise variations in the mean flow mediate an energy transfer between the forced mode and the eigenmode, resulting in a net receptivity. After presenting the problem formulation and perturbation method, we briefly describe the numerical method. The results focus on a two-dimensional wavy surface. These results provide the basis for a discussion of the receptivity mechanism and its principal effects on the disturbance evolution.

2. Problem formulation

We consider the acoustic receptivity of a boundary layer over a flat plate with non-localized two-dimensional surface irregularities. A schematic of the problem is given in figure 1. The fluid is assumed to be incompressible, so the acoustic wavenumber is zero. Both the acoustic amplitude and the height of the surface perturbation are assumed to be small. The base flow is a one-dimensional Blasius profile subject to the approximation of quasi-parallel flow. In the experiments of Reshotko & Leventhal (1981), no measurable deviation from the Blasius mean-flow profile was observed for flows over roughness of small height.

The quasi-parallel-flow approximation leads to an Orr–Sommerfeld type equation governing the disturbances. The weak streamwise variations are accounted for in a discrete manner, but the streamwise divergence terms are neglected. Numerical simulations for linear stability have demonstrated that Orr–Sommerfeld solutions give excellent estimates for disturbance profiles and growth rates (Fasel & Konzelmann 1990). The results for the quasi-parallel flow represent the lowest-order solutions for the non-parallel boundary layer (Gaster 1974; Saric & Nayfeh 1975).
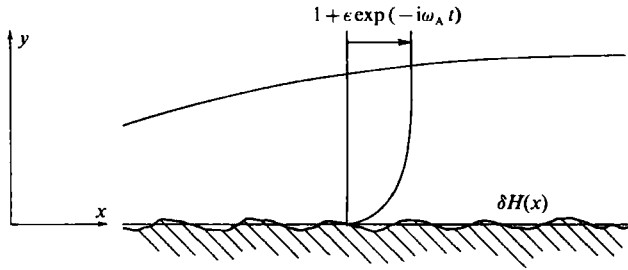
FIGURE 1. Schematic of problem formulation.

The flow is governed by the Navier–Stokes equations which we write in the form of a generalized nonlinear Orr–Sommerfeld equation. Starting with the vorticity transport equation, we take $\partial/\partial x$ of the spanwise-vorticity equation and subtract $\partial/\partial z$ of the streamwise-vorticity equation to yield

$$\mathbf{L}[v] + \mathbf{N}[v, v] = 0, \tag{1}$$

with

$$\mathbf{L}[v] = \left(\frac{1}{R_f} \nabla^2\right) \nabla^2 v - \frac{\partial}{\partial t} \nabla^2 v,$$

$$\mathbf{N}[v, v] = -\frac{\partial}{\partial x}(v \cdot \nabla)\zeta,$$

where $\boldsymbol{\omega} = \nabla \times v = (0, 0, \zeta)$ and $v = (u, v, 0)$. The coordinates (x, y, z) represent the streamwise, surface normal, and spanwise directions, respectively. All quantities are non-dimensionalized using the outer velocity, U_∞, and the fixed reference length $\delta_{rf} = \delta_r(\tilde{x}_f) = (\nu \tilde{x}_f/U_\infty)^{\frac{1}{2}}$. This results in a fixed Reynolds number $R_f = U_\infty \delta_{rf}/\nu$ which is related to the streamwise-varying Reynolds number $R = U_\infty \delta_r/\nu$ through the relation $R/R_f = \delta_r/\delta_{rf}$. All calculations are based on the reference Reynolds number $R_f = 1000$.

At the outer edge of the boundary layer the flow must match the free stream with the acoustic perturbation

$$u \to 1 + \epsilon \exp(-i\omega_A t) \quad \text{as} \quad y \to \infty. \tag{2}$$

The boundary condition at the wall is

$$u = v = 0 \quad \text{at} \quad y = \delta H(x). \tag{3}$$

The small parameters ϵ and δ characterize the amplitude of the acoustic forcing and the height of the irregularity, respectively. Any surface irregularity can be decomposed into a collection of Fourier components. To study the basic mechanisms for the non-localized generation of disturbances in the boundary layer, we consider a single-mode wavy wall

$$H(x) = \exp(i\alpha_w x), \tag{4}$$

where $\alpha_w = 2\pi/\lambda_w$ and λ_w is a characteristic wavelength of the surface perturbation.

In general, a single-frequency boundary-layer disturbance is described by a partial differential equation in x and y. We formulate the solution to this partial differential equation by decoupling the slow streamwise variation from the variation across the

boundary layer. Following the quasi-parallel-flow approximation we locally neglect the weak x variation and construct an ordinary differential equation in y. This nonlinear equation is reduced to a collection of linear problems using perturbation methods. The local x solutions are then used to construct an ordinary differential equation in x for the disturbance amplitude variation.

3. Perturbation analysis

We seek a solution of (1)–(3) in the form

$$v(x, y, t) = v_0(y;x) + \epsilon v_\epsilon(x, y, t) + \delta v_\delta(x, y, t) + \epsilon\delta v_{\epsilon\delta}(x, y, t), \tag{5}$$

where $v_0(y;x)$ is the local Blasius profile at the streamwise location x. The second-order functions ϵ^2 and δ^2 are not included in (5) since they do not contribute to the receptivity at this order. Streamwise variations of the boundary layer are accounted for by stretching the Blasius profile from $v_0(y_B)$ into $v_0(y;x)$, where $y_B = \tilde{y}/\delta_r$. This is analogous to the physical problem in which the profile changes, and other parameters like the wavenumber α_w remain constant. Using a Taylor expansion about $v(x, 0, t)$, the boundary condition (3) is moved from $y = \delta H$ to $y = 0$. Substituting (4) and (5) into (1)–(3) and collecting coefficients of like powers in ϵ and δ yields

Order ϵ:

$$L_0[v_\epsilon] = 0, \tag{6}$$

$$u_\epsilon \rightarrow \exp(-i\omega_A t) \quad \text{as} \quad y \rightarrow \infty, \tag{7}$$

$$u_\epsilon = v_\epsilon = 0 \quad \text{at} \quad y = 0, \tag{8}$$

Order δ:

$$L_0[v_\delta] = 0, \tag{9}$$

$$u_\delta \rightarrow 0 \quad \text{as} \quad y \rightarrow \infty, \tag{10}$$

$$u_\delta = -\frac{\partial u_0}{\partial y}\exp(i\alpha_w x), \quad v_\delta = 0 \quad \text{at} \quad y = 0, \tag{11}$$

Order $\epsilon\delta$:

$$L_0[v_{\epsilon\delta}] = -N[v_\epsilon, v_\delta] - N[v_\delta, v_\epsilon], \tag{12}$$

$$u_{\epsilon\delta} \rightarrow 0 \quad \text{as} \quad y \rightarrow \infty, \tag{13}$$

$$u_{\epsilon\delta} = -\frac{\partial u_\epsilon}{\partial y}\exp(i\alpha_w x), \quad v_{\epsilon\delta} = -\frac{\partial v_\epsilon}{\partial y}\exp(i\alpha_w x) \quad \text{at} \quad y = 0. \tag{14}$$

For stability analysis, $v_0(y;x)$ is considered known. Therefore, we introduce a new linear operator $L_0[v] = L[v] + N[v_0, v] + N[v, v_0]$. The disturbance velocities described by (6)–(14) are similar to the velocity components involved in the localized receptivity analyses of Goldstein (1985) and Kerschen (1989).

The problems (6)–(8) and (9)–(11) are linear with a homogeneous boundary condition at one boundary and an inhomogeneous condition at the other. We write the solution of (6)–(8) as

$$v_\epsilon(x, y, t) = v_A(y;x)\exp(-i\omega_A t). \tag{15}$$

This velocity component satisfies the free-stream acoustic boundary condition and a homogeneous wall boundary condition. Physically, it represents the Stokes flow

induced by an acoustic wave of frequency ω_A and zero grazing angle (Lighthill 1954). The v component of v_A is zero owing to the assumption of quasi-parallel flow, resulting in $v_A = (u_A, 0, 0)$. The solution of (9)–(11) is written as

$$v_\delta(x, y, t) = v_w(y; x) \exp{(i\alpha_w x)}, \tag{16}$$

which satisfies the wall boundary condition and a homogeneous free-stream condition. This corresponds to a wavy-wall mode which is a spatially-periodic standing wave (Lessen & Gangwani 1976). The two modes v_ϵ and v_δ are distinguished from eigensolutions since ω_A and α_w are real and cannot satisfy the characteristic equation.

Substituting the velocities (15) and (16) into (12)–(14) produces a set of equations for the mode generated by the nonlinear operator N. Equation (12) becomes

$$\mathbf{L}_0[v_{\epsilon\delta}] = \left[-i\alpha_w v_w \frac{\partial^2 u_A}{\partial y^2} + \alpha_w^2 \left(\frac{\partial u_w}{\partial y} - i\alpha_w v_w \right) u_A \right] \exp{[i(\alpha_w x - \omega_A t)]}. \tag{17}$$

This mode represents a travelling-wave disturbance resulting from the interaction of the Stokes mode and the wall mode. The corresponding boundary conditions are

$$u_{\epsilon\delta} \to 0 \quad \text{as} \quad y \to \infty, \tag{18}$$

$$u_{\epsilon\delta} = -\frac{\partial u_A}{\partial y} \exp{[i(\alpha_w x - \omega_A t)]}, \quad v_{\epsilon\delta} = 0 \quad \text{at} \quad y = 0. \tag{19}$$

$\mathbf{L}_0$, in (17), is the linear Orr–Sommerfeld operator. The complete spectral characteristics of this operator are still not fully understood. However, for the current analysis we will focus on a single discrete eigenmode corresponding to the most unstable disturbance. We consider forcing parameters (α_w, ω_A) which are close to the natural eigenmode parameters $(\alpha_{TS}, \omega_{TS})$. The right-hand side of (17) then provides a near-resonant forcing. As a result of resonance, energy is 'leaked' into the eigenmode leading to non-localized receptivity.

The solution to (17)–(19) is given by the superposition of a 'forced mode' (particular solution) $v_{\epsilon\delta F}$ and an eigenmode $v_{\epsilon\delta TS}$,

$$v_{\epsilon\delta} = v_{\epsilon\delta F} + v_{\epsilon\delta TS}. \tag{20}$$

To clarify the relationship between these modes (and the mechanism for receptivity) we focus on the streamwise velocity component $u_{\epsilon\delta}$. The forced mode has the form

$$u_{\epsilon\delta F} = \bar{A}_F(x)\, \bar{u}_F(y; x) \exp{[i\phi_F(y; x) + i\psi_F(x)]} \exp{[i\alpha_w x - i\omega_A t]}. \tag{21}$$

We define the response amplitude $\bar{A}_F = \max|u_F|$ as a measure of the magnitude of the response. The variation of u_F across the boundary layer is described by the normalized magnitude profile $\bar{u}_F$ and the phase profile ϕ_F. The response phase ψ_F is the result of requiring ϕ_F to be zero at the location of the maximum of the $\bar{u}_F$ profile. The functions $\bar{A}_F$, $\bar{u}_F$, ϕ_F, and ψ_F are all calculated locally but depend weakly on x. A TS eigenmode with the same fixed frequency is given by

$$u_{\epsilon\delta TS} = \bar{A}_{TS}(x)\, \bar{u}_{TS}(y; x) \exp{[i\phi_{TS}(y; x) + i\psi_{TS}(x)]} \exp{\left[i \int_{x_0}^{x} \alpha_{TSr}(s)\, ds - i\omega_A t \right]}, \tag{22}$$

where x_0 is some upstream reference location. The functions $\bar{A}_{TS}$, $\bar{u}_{TS}$, ϕ_{TS}, and ψ_{TS} all depend weakly on x, or R. The imaginary part of α_{TS} is incorporated in the amplitude $\bar{A}_{TS}$.

The streamwise-velocity component of the total travelling-wave disturbance with frequency ω_A is given by the sum of (21) and (22)

$$u_{\epsilon\delta} = A(x)\exp[i\psi(x)]\bar{u}(y;x)\exp[i\phi(y;x)]\exp[-i\omega_A t] = u_{\epsilon\delta F} + u_{\epsilon\delta TS}. \quad (23)$$

The streamwise variation of the total disturbance is described by the amplitude A and phase ψ. The variation across the boundary layer is given by the normalized profile $\bar{u}$ and phase ϕ. For the near-resonant conditions needed for receptivity, the forced mode profile has the same shape as the eigenmode except in a thin region near the wall (this is demonstrated in §5). The total disturbance, being the sum of $u_{\epsilon\delta F}$ and $u_{\epsilon\delta TS}$, also exhibits the eigenmode shape. As a result of these profile similarities, the streamwise variation described by (23) can be simplified to an amplitude equation. The total travelling-wave disturbance at frequency ω_A is then characterized by

$$A(x)\exp[i\psi(x)] = \Lambda_F(x)\exp[i\alpha_w(x-x_0)] + A_{TS}(x)\exp\left[i\int_{x_0}^x \alpha_{TSr}(s)\,ds\right], \quad (24)$$

where $\Lambda_F = \bar{\Lambda}_F\exp(i\psi_F)$ and $A_{TS} = \bar{A}_{TS}\exp(i\psi_{TS})$ are complex amplitudes. The eigenmode amplitude A_{TS} can contain variation from both linear growth and the forced mode.

4. Amplitude evolution equation

Having formulated the local solution for any given x, we now relax the parallel-flow assumption in order to develop a streamwise representation of the disturbance. This is the standard quasi-parallel-flow approach which is the lowest-order solution for the stability of a weakly non-parallel boundary layer (Gaster 1974; Saric & Nayfeh 1975). Taking the derivative with respect to x of (24) yields

$$\left(\frac{dA}{dx} + iA\frac{d\psi}{dx}\right)\exp[i\psi] = \left(\frac{dA_{TS}}{dx} + i\alpha_{TSr}A_{TS}\right)\exp\left[i\int_{x_0}^x \alpha_{TSr}(s)\,ds\right]$$
$$+ \left(\frac{d\Lambda_F}{dx} + i\alpha_w\Lambda_F\right)\exp[i\alpha_w(x-x_0)]. \quad (25)$$

Variations of the amplitudes occur on a 'large' streamwise lengthscale relative to the periodic terms which vary on the 'small' scale of the instability wavelength. This scaling is implicit in any normal-mode type analysis. Balancing the small lengthscale terms in (25) gives

$$iA\frac{d\psi}{dx}\exp[i\psi] = i\alpha_{TSr}A_{TS}\exp\left[i\int_{x_0}^x \alpha_{TSr}(s)\,ds\right] + i\alpha_w\Lambda_F\exp[i\alpha_w(x-x_0)]. \quad (26)$$

This equation implies that the variation of the total phase is dominated by the periodic variation of the forced mode and the eigenmode. The large lengthscale variations are given by

$$\frac{dA}{dx}\exp[i\psi] = \frac{dA_{TS}}{dx}\exp\left[i\int_{x_0}^x \alpha_{TSr}(s)\,ds\right] + \frac{d\Lambda_F}{dx}\exp[i\alpha_w(x-x_0)]. \quad (27)$$

We now decompose the eigenmode-amplitude variation into a linear-growth term and a term resulting from the energy exchange with the forced mode

$$\frac{dA_{TS}}{dx} = -\alpha_{TSi}A_{TS} + F. \quad (28)$$

The function $F(x)$ describes the influence of the forced mode, and is as yet unknown. Substituting (28) into (27) gives

$$\frac{\mathrm{d}A}{\mathrm{d}x}\exp\left[\mathrm{i}\psi\right] = (-\alpha_{\mathrm{TSi}}A_{\mathrm{TS}} + F)\exp\left[\mathrm{i}\int_{x_0}^{x}\alpha_{\mathrm{TSr}}(s)\,\mathrm{d}s\right] + \frac{\mathrm{d}A_{\mathrm{F}}}{\mathrm{d}x}\exp\left[\mathrm{i}\alpha_{\mathrm{w}}(x-x_0)\right]. \quad (29)$$

During a passage through near-resonant conditions, the forced-mode amplitude varies more rapidly than the normal eigenmode-amplitude variation of $\alpha_{\mathrm{TSi}}A_{\mathrm{TS}}$ (this is demonstrated in §5). This rapid variation of A_{F} in (29) can lead to large values of A which would result in a non-uniform velocity expansion. We determine F by requiring the expansion for v to be uniform over the range of x being considered. From (29), this requirement leads to

$$F(x) = -\frac{\mathrm{d}A_{\mathrm{F}}}{\mathrm{d}x}\exp\left[\mathrm{i}\alpha_{\mathrm{w}}(x-x_0) - \mathrm{i}\int_{x_0}^{x}\alpha_{\mathrm{TSr}}(s)\,\mathrm{d}s\right]. \quad (30)$$

Equation (30) can be considered as a balance of terms which vary on an 'intermediate' lengthscale (which is large compared to the disturbance wavelength, but small compared to the lengthscale of the normal eigenmode-amplitude variation). Substituting for F in (28) then provides a differential equation for the eigenmode amplitude

$$\frac{\mathrm{d}A_{\mathrm{TS}}}{\mathrm{d}x} = -\alpha_{\mathrm{TSi}}A_{\mathrm{TS}} - \frac{\mathrm{d}A_{\mathrm{F}}}{\mathrm{d}x}\exp\left[\mathrm{i}\alpha_{\mathrm{w}}(x-x_0) - \mathrm{i}\int_{x_0}^{x}\alpha_{\mathrm{TSr}}(s)\,\mathrm{d}s\right]. \quad (31)$$

The forced mode provides energy to the eigenmode in proportion to its rate of streamwise variation. This growth modification is scaled by the difference in phase between the forced mode with α_{w} and the eigenmode with α_{TSr}. Far from resonance, $A_{\mathrm{F}}(x)$ varies slowly and contributes only weakly to the eigenmode. Near resonance, $A_{\mathrm{F}}(x)$ changes more rapidly with x and dominates the eigenmode variation.

Following the scaling arguments described above, we can construct a finite-difference equation equivalent to (31). Using this approach, the energy transfer into the eigenmode is seen to result from the continuous projection of the total disturbance onto the slowly-varying forced and eigenmode solutions. This method of calculating the eigenmode amplitude has also been successfully applied to a much simpler model problem. We have considered a forced harmonic oscillator with slowly varying natural frequency (analogous to the eigenmode wavenumber). Using a theoretical expression (similar to (31)) for the amplitude and phase, the total response can be generated. The theory is in complete agreement with direct numerical integration of the original differential equation. This model problem and the finite difference approach are discussed in the Appendix.

An initial amplitude is required to determine the eigenmode evolution from (31). At some distance sufficiently far upstream the eigenmode amplitude will be zero, if no other form of receptivity is involved. Solving (31) for A_{TS}, with the initial condition $A_{\mathrm{TS}}(x_0) = 0$, gives

$$A_{\mathrm{TS}}(x) = -\int_{x_0}^{x}\frac{\mathrm{d}A_{\mathrm{F}}}{\mathrm{d}\hat{x}}\exp\left[\mathrm{i}\alpha_{\mathrm{w}}(\hat{x}-x_0) - \mathrm{i}\int_{x_0}^{\hat{x}}\alpha_{\mathrm{TSr}}(s)\,\mathrm{d}s - \int_{\hat{x}}^{x}\alpha_{\mathrm{TSi}}(s)\,\mathrm{d}s\right]\mathrm{d}\hat{x}. \quad (32)$$

Selection of the initial streamwise location x_0 for evaluating the eigenmode amplitude is based on numerical experiments.

The evaluation of (31) for the conditions of perfect resonance requires some special consideration. Under these conditions A_{F} tends to infinity with a phase shift of π radians at branch I. As a result, $\mathrm{d}A_{\mathrm{F}}/\mathrm{d}x$ also tends to infinity and is discontinuous

at branch I. Equation (32) must then be decomposed into an integral to the left of branch I and an integral to the right of branch I with an additional contribution from the jump discontinuity. When solving (32) numerically, this decomposition occurs naturally as a result of the discretization.

The perturbation analysis, in conjunction with the quasi-parallel-flow approximation, reduces the original equations (1)–(3) to sets of linear ordinary differential equations. These equations are solved using a spectral collocation method. The unbounded domain $y \in [0, \infty)$ is transformed into the bounded domain $\eta \in [1, 0)$ using the algebraic mapping $\eta = \eta_0/(y + \eta_0)$. The parameter η_0 controls the distribution of points across the boundary layer. Odd Chebyshev polynomials are used as expansion functions that automatically satisfy homogeneous boundary conditions at infinity. The presented results are based on 30 collocation points and $\eta_0 = 4.5$, which positions half of the collocation points within the displacement thickness of the boundary layer.

5. Travelling wave: forced-mode and eigenmode response

We now consider the $O(\epsilon\delta)$ travelling-wave solution given by (21) and (22). This solution contains both a forced mode and an eigenmode. For receptivity analysis we focus on the most unstable eigenmode. We first consider the forced travelling-wave mode which is the particular solution of (17)–(19). The evolution of the natural eigenmode is then discussed.

A forced travelling-wave generated over a wavy surface is described by the parameters $F = 10^6 \, \omega_A/R_f$ and α_w which remain constant with changing Reynolds number R. A TS eigenmode of fixed frequency ω_A, on the other hand, is characterized by a slowly changing (complex) wavenumber α_{TS} determined by the dispersion relation. If we track an eigenmode of fixed frequency downstream, the mode may coincide with the forced mode ($\alpha_{TSr} = \alpha_w$) at some Reynolds number R^*. Figure 2 shows the wavenumber variation for an eigenmode of fixed frequency $F = 56$ and a forced mode corresponding to $R^* = 550$.

The condition of $\alpha_w \approx \alpha_{TSr}$, where (F, α_{TS}) are the local TS parameters, permits the forced mode to act as a seeding for the local eigenmode disturbance. The details of the seeding mechanism will depend on the particular value of α_w. For the special case of $\alpha_w = \alpha_{TSr}$ at a neutral point (where the imaginary $\alpha_{TSi} = 0$), a perfect resonance occurs between the right-hand-side forcing of (17) and the homogeneous eigenmode solution. Thus when the forced mode parameters are numerically identical to the branch I TS parameters the response at $R = R^*$ is singular.

A more typical response is obtained by considering an R^* value away from the neutral point. A small variation in α_w, away from the special condition $\alpha_w = \alpha_{TS}$ at branch I, introduces detuning between the forcing and the natural oscillation. This eigenvalue detuning ($\alpha_w \neq \alpha_{TSr}$ at branch I, and $\alpha_{TSi} \neq 0$ at R^*) removes the singular behaviour, analogous to the addition of damping in a linear forced-vibration system. For R^* away from branch I, the maximum response is reduced and is shifted in Reynolds number from branch I toward R^*. The maximum response, however, is still in the neighbourhood of branch I (where $\alpha_{TSi} \approx 0$) and not near R^* (where $\alpha_w \approx \alpha_{TSr}$). This results from the detuning of $\alpha_{TSr} - \alpha_w$ near branch I being smaller than the detuning of α_{TSi} near R^* as shown in figure 2.

Having the forced response at $(F, \alpha_w; x)$, we can determine the eigenmode response at $(F, \alpha_{TSr}; x)$ from (32). The combination of these two modes then provides the total travelling-wave disturbance. To facilitate comparisons with experiments, we
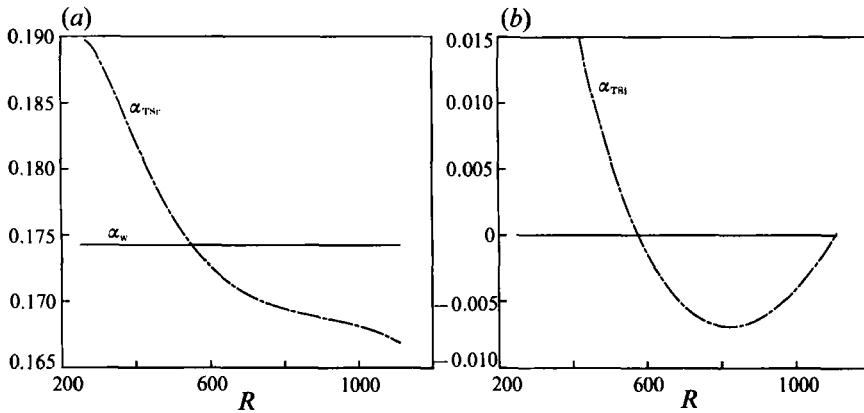
FIGURE 2. Streamwise variation of the (a) real α_{TSr} and (b) imaginary α_{TSi} parts of the eigenmode wavenumber α_{TS} for $F = 56$. The forced-mode wavenumber for $R^* = 550$ is given for comparison.
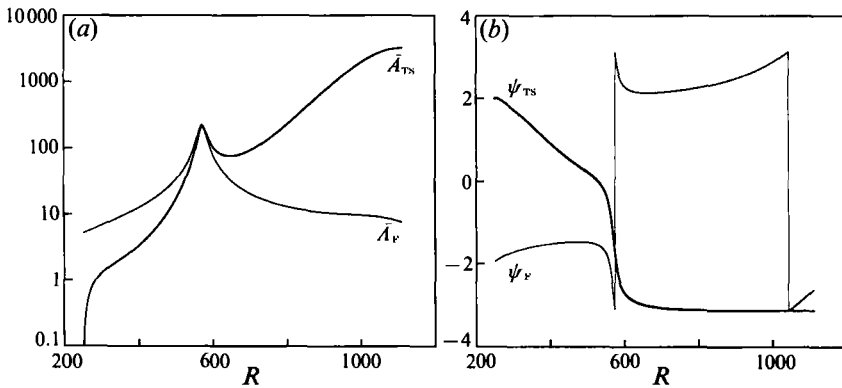
FIGURE 3. Streamwise variation of the eigenmode (a) amplitude and (b) phase superposed on the forced-mode response at $F = 56$, $\alpha_w = 0.174236$, $R^* = 550$.

introduce the Reynolds number R as the independent variable. The streamwise location x is related to R through the expression $x = \tilde{x}\delta_{rf} = R^2/R_f$. Figure 3 shows the variation of the eigenmode amplitude and phase in conjunction with the corresponding forced mode for $F = 56$, $\alpha_w = 0.174236$ ($R^* = 550$). The forced mode shows a strong peak near branch I, $R \approx 576$. Away from branch I the forced response drops off by more than an order of magnitude. The forced-mode phase also undergoes dramatic variation in the region of near resonance. Meanwhile, the streamwise development of the eigenmode is characterized by three distinct stages. During the first stage, contributions from the forced mode are small owing to $dA_F/dx \ll 1$. Initially the eigenmode amplitude increases rapidly from an initial upstream value of zero, but once the eigenmode reaches an amplitude of $O(1)$ at $R \approx 300$ it grows at a nearly constant rate. During the second stage of development, the energy transfer between the forced mode and the eigenmode increases dramatically. This energy transfer is tied to large values of dA_F/dx over the region $R \approx 400$ to $R \approx 700$. The rapid changes in A_F are due to the near resonant response of the forced mode. Simultaneously with the strong energy transfer, the eigenmode phase undergoes a shift of approximately π radians. During the third stage, contributions from the forced mode are again small and the eigenmode evolution is governed by its linear growth characteristics. The eigenmode phase ψ_{TS} then takes on a constant value.
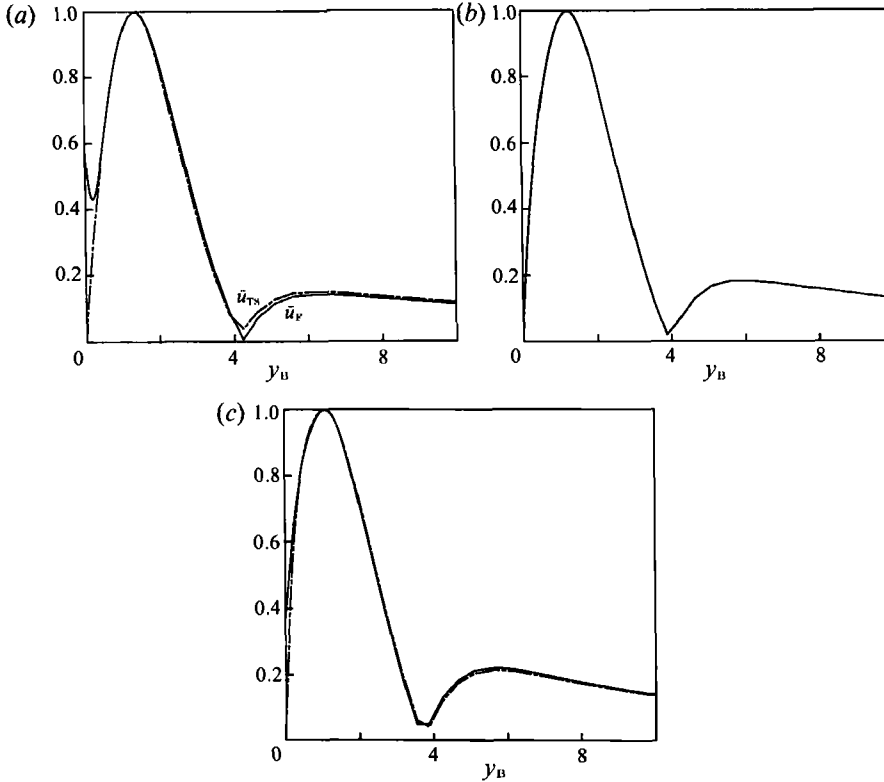
FIGURE 4. Normalized u velocity profiles for the forced mode and the eigenmode at (a) $R = 400$, (b) $R = 550$, and (c) $R = 700$. Results for $F = 56$, $\alpha_w = 0.174236$, $R^* = 550$.

A sequence of normalized streamwise-velocity profiles for the conditions of figure 3 are given in figure 4. In general, the forced mode profile is very similar to the corresponding TS profile. At $R = 400$, the forced mode profile shows a distinct deviation from the TS profile near the wall owing to the inhomogeneous boundary condition. At $R = 550$, the maximum of the TS profile is closer to the wall and the forced mode response is increased, thus reducing the deviation between the profiles. Downstream of branch I at $R = 700$, the forced profile again shows some deviation from the TS profile near the wall. However, the deviation is small because of the shift of the TS maximum toward the wall. Near the region of the profile maximum, the forced mode profiles are in very close agreement with the eigenmode for each of the streamwise locations. Phase profiles for these conditions also show very close agreement between the forced mode and the eigenmode, except for a thin region near the wall.

6. Travelling wave: total response

The principal goal of a receptivity study is usually to provide initial values for eigenmode amplitudes in terms of free-stream disturbances and characteristics of the surface irregularity. However, for non-localized receptivity the total travelling-wave disturbance, including both the forced mode and the eigenmode, must be considered. The total disturbance provides the physically relevant solution for the problem.

The total disturbance amplitude A, measurable in an experiment, is obtained from (24) using A_{TS} and A_F. Figure 5 shows the total disturbance evolution for the
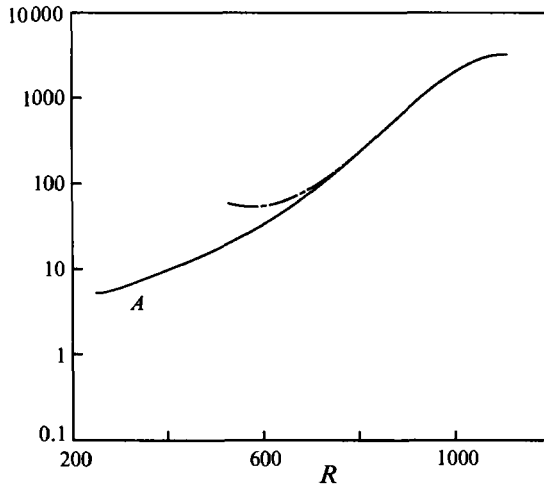
FIGURE 5. Streamwise variation of the total amplitude at $F = 56$, $\alpha_w = 0.174236$, $R^* = 550$. The linear growth curve is given for comparison.

conditions of figure 3. The dashed line represents a linear growth curve obtained by matching the total disturbance amplitude at branch II. After an initial adjustment from $A = \bar{A}_F$ at R_0 (the Reynolds number corresponding to x_0), the total disturbance amplitude grows at an almost constant rate between $R \approx 300$ and $R \approx 450$. The growth of A then increases over the region of large forced-mode response. This is the period of strongest energy transfer between the forced mode and the eigenmode. As the forced mode amplitude diminishes, the eigenmode dominates the total disturbance.

An interesting feature of the total amplitude evolution is the large effective growth rate. Effective growth rates can be even greater for multiple wavy-wall modes. The largest deviation between the effective growth rate and the linear growth rate occurs in the neighbourhood (and upstream) of branch I where the forced-mode response is maximal. This is in qualitative agreement with experiments of Corke *et al.* (1986, figure 16) and Reshotko (1984, figures 4, 5, and 12). However, in the experiments of Reshotko, transition ultimately occurs as a result of some form of 'by-pass.' A quantitative comparison to these rough-wall experiments would require detailed spectral information about the surfaces and the free stream.

In order to compare the current results with results for other receptivity mechanisms we define an effective branch I amplitude A_I. This is obtained by projecting the total amplitude at branch II back to branch I using the appropriate N-factor. The effective branch I amplitude recasts the total distributed receptivity into a single-amplitude value at one particular streamwise location (branch I). For the conditions of figure 5, $A_I = 53.7$.

The results of figures 3 and 5 are based on calculating the eigenmode amplitude from the initial Reynolds number $R_0 = 250$. To justify $R_0 = 250$ as sufficiently far upstream, we consider the effect of R_0 on the calculation of the effective branch I amplitude A_I. Figure 6 shows the variation of A_I with R_0 for the conditions $F = 56$, $R^* = 550$. For R_0 values between 450 and 700 the effective receptivity is very sensitive to R_0. This is the principal region of energy transfer into the eigenmode. If R_0 is upstream of this region, the total energy transfer is captured and the effective branch I amplitude is independent of R_0. The effective branch I amplitude changes less than 0.02% between $R_0 = 250$ and $R_0 = 300$. For R_0 values downstream of
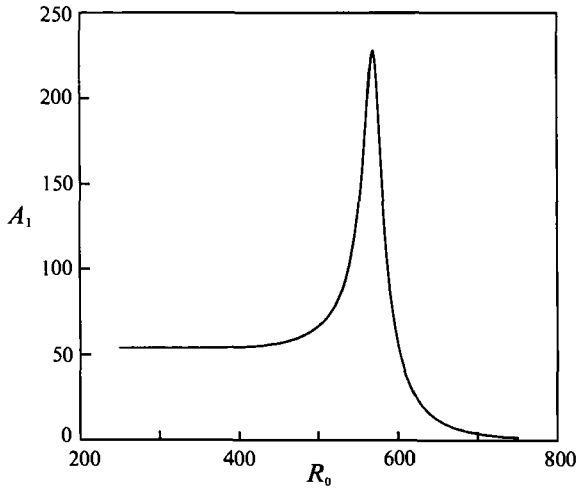
FIGURE 6. Variation of the effective branch I amplitude A_1 with R_0 for the conditions $F = 56$ and $R^* = 550$.
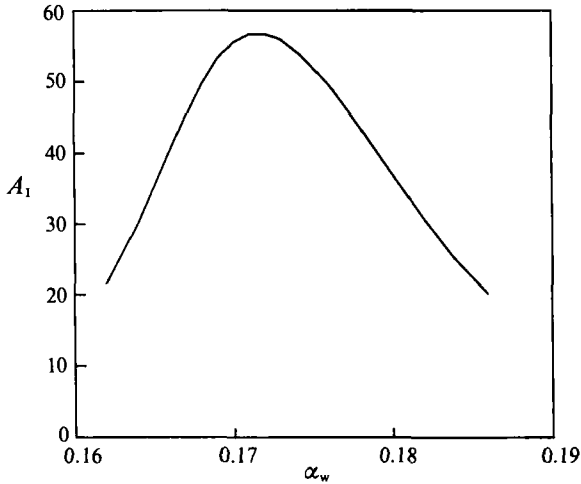
FIGURE 7. Variation of the effective branch I amplitude A_1 with α_w for the conditions $F = 56$ and $R_0 = 250$.

$R \approx 700$, the principal energy transfer is not captured and A_I tends to zero as R_0 increases. The results of figure 6 suggest that any $R_0 < 300$ is sufficiently far upstream. Figure 6 does not represent the receptivity resulting from surface variations having a distinct beginning. To calculate the receptivity over such a surface the localized end contribution $(A_{TS}(x_0) \neq 0)$ must also be considered. This end contribution balances the large response for $400 < R_0 < 700$ resulting in a monotonic decrease in A_I as R_0 increases beyond $R \approx 300$.

Calculations of the effective branch I amplitudes for different values of the wavenumber α_w are given in figure 7. The largest receptivity occurs for wavenumbers corresponding to R^* values between branch I ($\alpha_w \approx 0.173$) and branch II ($\alpha_w \approx 0.167$). However, the mechanism is operative over a broad band of wavenumbers. For wavenumbers below $\alpha_w \approx 0.168$ the eigenmode is still gaining energy from the forced mode at branch II. Non-localized receptivity produces disturbances one-to-

two orders of magnitude greater than localized receptivity as expressed in terms of branch I amplitudes (Kerschen 1989; Goldstein & Hultgren 1989). Such a strong mechanism requires only mild surface waviness to produce significant receptivity. Rough surfaces, with variations in the roughness height, will be extremely susceptible to this mechanism.

To assess the effects of the quasi-parallel and lengthscale assumptions, the parabolized stability equations (PSE) (Herbert & Bertolotti 1987; Bertolotti, Herbert & Spalart 1990) are being used to study the receptivity over a wavy wall.† The PSE are nonlinear partial differential equations that incorporate the effects of streamwise divergence associated with the boundary-layer non-parallelism. The equations are solved numerically by a streamwise marching procedure which permits the capture of the receptivity directly, without explicitly calculating all of the modes considered in the theory. The effective branch I amplitude calculated from the PSE, for the conditions of figure 5, is $A_1 = 51.7$ compared to the theoretical value of $A_I = 53.7$. This good agreement lends support to the theoretical model and suggests that the approximations are well founded and not overly restrictive.

7. Summary and conclusions

Using perturbation analysis, we have constructed a non-localized receptivity theory which includes a scale-reduction mechanism necessary for acoustic receptivity. The Blasius mean flow over a surface with small-amplitude waviness produces a wall mode that is periodic in space and fixed in time. Acoustic perturbations in the free stream modulate this disturbance field to produce a travelling wave which scales linearly with both the acoustic forcing and the height of the surface waviness. The travelling wave is composed of an eigenmode and a forced mode. Streamwise variations in the mean flow activate a distributed energy transfer between these modes. This energy transfer is maximized in the neighbourhood of branch I where the forced response is most significant. Downstream of the strong energy transfer the forced-mode amplitude is small, leaving the eigenmode as the dominant component of the total disturbance. Projecting the disturbance amplitude back to branch I provides an effective receptivity amplitude. The branch I receptivity amplitudes A_I are $O(10)$ over a broad range of surface wavenumbers. When operative, this will be a dominant mechanism for boundary-layer receptivity.

Appendix

We consider a forced harmonic oscillator as a model problem to help demonstrate the approach for calculating the eigenmode amplitude. The equation governing a forced oscillator, with varying natural frequency is

$$\mathrm{d}^2 u / \mathrm{d} x + \omega^2(x)\, u = \cos \Omega x \qquad \text{(A 1)}$$

† Work done in conjunction with F. P. Bertolotti.
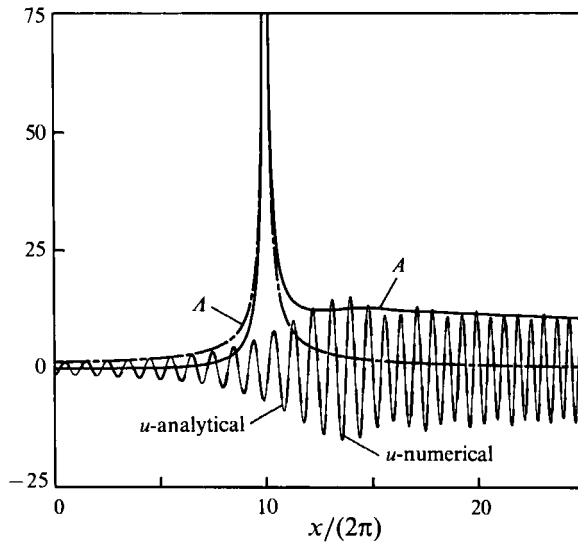
FIGURE 8. Variation of the total solution u, and the forced and eigenmode amplitudes for the model problem. Resonance occurs at $x/2\pi = 10$.

where ω varies slowly with x. The 'local' solution of (A 1) for fixed ω is given by

$$u(x) = A\cos{(\omega x + \beta)} + \varLambda\cos{\varOmega x}, \qquad (A\ 2)$$

where $\varLambda = 1/(\omega^2 - \varOmega^2)$, with A and β determined by initial conditions. To formulate an expression for the variation of A, we follow a finite-difference approach (rather than the differential approach used in §4). This provides some additional insights into the mechanism of energy transfer into the eigenmode. Assuming the complete solution is known at x_1, we can calculate an approximate solution at $x_2 = x_1 + \Delta x$ by allowing only the 'fast' periodic terms to vary. A local calculation at x_2 then provides a general solution in the form of (A 2). The eigenmode amplitude and phase at x_2 are determined by using the approximate solution as an initial value. This yields the desired expressions for the amplitude and phase

$$A_2^2 = [A_1\cos{(\omega_1 x_2 + \beta_1)} - (\varLambda_2 - \varLambda_1)\cos{\varOmega x_2}]^2$$
$$+ \left[\frac{\omega_1}{\omega_2}A_1\sin{(\omega_1 x_2 + \beta_1)} - \frac{\varOmega}{\omega_2}(\varLambda_2 - \varLambda_2)\sin{\varOmega x_2}\right]^2, \quad (A\ 3)$$

$$\beta_2 = \tan^{-1}\left[\frac{\omega_1 A_1\sin{(\omega_1 x_2 + \beta_1)} - (\varLambda_2 - \varLambda_1)\varOmega\sin{\varOmega x_2}}{\omega_2(A_1\cos{(\omega_1 x_2 + \beta_1)} - (\varLambda_2 - \varLambda_1)\cos{\varOmega x_2})}\right] - \omega_2 x_2, \qquad (A\ 4)$$

where the subscripts 1 and 2 signify the values at x_1 and x_2, respectively. Given the initial conditions at some location x_0, the eigenmode response is calculated using (A 3) and (A 4). Substituting for the eigenmode amplitude and phase in (A 2) then yields the total solution. Variation in x leads to a change in ω and $\varLambda$ which in turn require a continuous adjustment of the eigenmode response.

As an example, we consider the case $\omega = 0.5 + 0.05(x/2\pi), \varOmega = 1$. The initial conditions are $u(0) = \varLambda(0), u'(0) = 0$, which is equivalent to setting $A(0) = 0$. Figure 8 shows the results from both the analysis and a direct numerical integration of (A 1). The analytical value for u is indistinguishable from the numerical result. The forced mode and the eigenmode amplitudes are also shown. As ω passes through

resonance ($\omega = \Omega$ at $x/2\pi = 10$), the forced-mode amplitude tends to infinity. The eigenmode amplitude follows the forced mode through resonance, but the two modes are approximately 180° out of phase. Meanwhile, the total amplitude grows at a rate proportional to x, as expected for resonance. Prior to resonance (say, $x/2\pi < 5$), $A \approx 0$ and u varies with the forced frequency Ω. After resonance, A tends to zero and A tends to a constant value. The total solution then varies with the natural frequency ω. During resonance the solution is non-stationary, being characterized by a combination of the forced and eigenmode responses.

REFERENCES

AIZIN, L. B. & POLYAKOV, M. F. 1979 Acoustic generation of Tollmien–Schlichting waves over local unevenness of surfaces immersed in streams. Preprint 17, Akad. Nauk USSR, Siberian Div., Inst. Theor. Appl. Mech., Novosibirsk (in Russian).

BERTOLOTTI, F. P., HERBERT, TH. & SPALART, P. R. 1992 Linear and nonlinear stability of the Blasius boundary layer. *J. Fluid Mech.* **242**, 441–474.

CORKE, T. C., BAR SEVER, A. & MORKOVIN, M. V. 1986 Experiments on transition enhancement by distributed roughness. *Phys. Fluids* **29**, 3199–3213.

FASEL, H. & KONZELMANN, U. 1990 Non-parallel stability of a flat-plate boundary layer using the complete Navier–Stokes equations. *J. Fluid Mech.* **221**, 311–347.

GASTER, M. 1974 On the effects of boundary-layer growth on flow stability. *J. Fluid Mech.* **66**, 465–480.

GOLDSTEIN, M. E. 1983 The evolution of Tollmien–Schlichting waves near a leading edge. *J. Fluid Mech.* **127**, 59–81.

GOLDSTEIN, M. E. 1985 Scattering of acoustic waves into Tollmien–Schlichting waves by small streamwise variations in surface geometry. *J. Fluid Mech.* **154**, 509–529.

GOLDSTEIN, M. E. & HULTGREN, L. S. 1987 A note on the generation of Tollmien–Schlichting waves by sudden surface curvature change. *J. Fluid Mech.* **181**, 519–525.

GOLDSTEIN, M. E. & HULTGREN, L. S. 1989 Boundary-layer receptivity to long-wave free-stream disturbances. *Ann. Rev. Fluid Mech.* **21**, 137–166.

HERBERT, TH. & BERTOLOTTI, F. P. 1987 Stability analysis of nonparallel boundary layers. *Bull. Am. Phys. Soc.* **32**, 2079.

KERSCHEN, E. J. 1989 Boundary layer receptivity. *AIAA paper* 89–1109.

LEEHEY, P. & SHAPIRO, P. J. 1980 Leading edge effect in laminar boundary layer excitation by sound. In *Laminar–Turbulent Transition, IUTAM Symposium, Stuttgart, Germany, September 1979* (ed. R. Eppler & H. Fasel), pp. 321–331. Springer.

LESSEN, M. & GANGWANI, S. T. 1976 Effect of small amplitude wall waviness upon the stability of the laminar boundary layer. *Phys. Fluids* **19**, 510–513.

LIGHTHILL, M. J. 1954 The response of laminar skin friction and heat transfer to fluctuations in the stream velocity. *Proc. R. Soc. Lond.* A **224**, 1–23.

MACK, L. M. 1975 Linear stability theory and the problem of supersonic boundary-layer transition. *AIAA J.* **13**, 278–289.

RESHOTKO, E. 1976 Boundary-layer stability and transition. *Ann. Rev. Fluid Mech.* **8**, 311–349.

RESHOTKO, E. 1984 Disturbances in a laminar boundary layer due to distributed roughness. In *Turbulence and Chaotic Phenomena in Fluids* (ed. T. Tatsumi), pp. 39–46. Elsevier.

RESHOTKO, E. & LEVENTHAL, L. 1981 Preliminary experimental study of disturbances in a laminar boundary layer due to distributed surface roughness. *AIAA paper* 81–1224.

ROGLER, H. L. & RESHOTKO, E. 1975 Disturbances in a boundary layer introduced by a low intensity array of vortices. *SIAM J. Appl. Maths* **28**, 431–462.

SARIC, W. S. & NAYFEH, A. H. 1975 Non-parallel stability of boundary layer flows. *Phys. Fluids* **18**, 945–950.

TAM, C. K. W. 1981 The excitation of Tollmien–Schlichting waves in low subsonic boundary layers by free-stream sound waves. *J. Fluid Mech.* **109**, 483–501.